Accurate control of Josephson phase qubits

Matthias Steffen,[1, 2, *] John M. Martinis,[3] and Isaac L. Chuang[1]

[1]*Center for Bits and Atoms - MIT, Cambridge, Massachusetts 02139*
[2]*Solid State and Photonics Laboratory, Stanford University, Stanford, CA 94305-4075*
[3]*National Institute of Standards and Technology, 325 Broadway, Boulder, CO 80305-3328*
(Dated: June 24, 2003)

A quantum bit is a closed two-dimensional Hilbert space, but often experimental systems have three or more energy levels. In a Josephson phase qubit the energy differences between successive levels differ by only a few percent, and hence care must be taken to isolate the two desired levels from the remaining Hilbert space. Here we show via numerical simulations how to restrict operations to the qubit subspace of a three-level Josephson junction system requiring shorter time duration and suffering less error compared with traditional methods. This is achieved by employing amplitude modulated pulses as well as carefully designed sequences of square wave pulses. We also show that tunneling out of higher lying energy levels represents a significant source of decoherence that can be reduced by tuning the system to contain four or more energy levels.

I. INTRODUCTION

The remarkable promise of quantum computation[1] has led to the invention of a significant number of proposals for building a practical and scalable quantum computer. Several of these proposals[2–5] envision the use of two out of several energy levels in a system as a quantum bit (qubit) and hence care must be taken to isolate these levels from the remaining Hilbert space. In particular, in a Josephson phase qubit[4,5], energy differences between successive levels only differ by a few percent. The challenge in performing accurate qubit operations lies in successfully isolating the two energy levels from the rest of Hilbert space. In other words, how is it possible to operate as quickly and with as little error as possible on the qubit subspace while isolating the remaining Hilbert space in a Josephson phase qubit? This is especially important when the coherence times of the system are short.

A Josephson phase qubit can be described by three energy levels $|0\rangle$, $|1\rangle$, and $|2\rangle$, with energies E_0, E_1, and E_2, as sketched in Fig. 1b. The qubit space is formed by $|0\rangle$ and $|1\rangle$, and hence we wish to operate only within this subspace. Clearly, the higher-order transition can be avoided when exciting the ω_{10} transition by using a long enough excitation duration. However, because one wants to maximize the number of logic operations within a fixed coherence time, there is a need to excite the $|0\rangle \leftrightarrow |1\rangle$ transition as quickly as possible without populating other states.

Here we numerically model two techniques which show how single-qubit operations can be improved beyond simple square wave pulses (or "hard" pulses). The first uses amplitude modulation of the pulse and the second uses composite pulses that consist of a sequence of specially designed hard pulses. Though other proposals are known[6–8] for implementing single-qubit rotations within a subspace of Hilbert space, this work takes a further step by analyzing decoherence effects; specifically, we evaluate the feasibility of our methods for typical parameters of a Josephson phase qubit, including the effects of tunneling out of higher lying energy levels. We show that these tunneling effects can be a significant source of decoherence if not taken into account properly.

The outline of the paper is as follows. We first review the physics of the Josephson phase qubit in section II. In section III, we provide a concrete procedure detailing our methods to simulate the effect of applying amplitude modulated pulses to the qubit. Our results indicate that Gaussian shaped modulation[9] provides the best selectivity. In section IV, we describe two composite pulses, which perform better than hard pulses, but not quite as well as Gaussian shaped pulses. In section V, we show how to include tunneling effects out of the higher energy levels to estimate the feasibility of these techniques in a real Josephson junction qubit system. Our results indicate that tunneling plays a significant role, leading to the conclusion that, to reduce tunneling effects one should use at least four energy levels instead of the usual three[5].

Though our methods have been developed in the context of Josephson phase qubits, we believe they could also be fruitful in other systems where one wishes to control a particular subspace of Hilbert space. This work takes first steps towards transferring ideas from Nuclear Magnetic Resonance (NMR) quantum computing[10], specifically shaped and composite pulses, to other proposals for implementing a quantum computer; we believe this to be a very rewarding approach. Furthermore, our analysis of the effects of tunneling uses ideas from quantum computing to give us an unusual and interesting way to understand and model the physics of a real Josephson junction qubit.

II. JOSEPHSON PHASE QUBITS

The details of a Josephson phase qubit are described elsewhere[11], and we review only the basics here. The Hamiltonian of the current-biased Josephson junction with bias source I, critical junction current I_0, and junc-
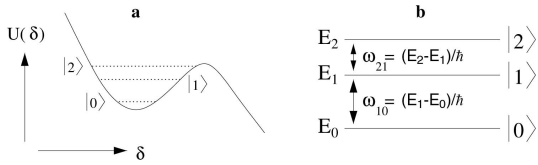
FIG. 1: Sketch of a three level system with two transitions at frequencies ω_{10} and ω_{21}.

tion capacitance C is

$$H = \frac{1}{2C}\hat{Q}^2 - \frac{I_0\Phi_0}{2\pi}\cos\hat{\delta} - \frac{I\Phi_0}{2\pi}\hat{\delta}, \qquad (1)$$

where $\Phi_0 = h/2e$ is the superconducting flux quantum. The operators $\hat{Q}$ and $\hat{\delta}$ correspond to the charge and the superconducting phase difference across the junction, respectively, and have a commutation relationship $[\hat{\delta},\hat{Q}] = 2ei$. Quantum mechanical behavior can be observed for large area junctions in which $I_0\Phi_0/2\pi = E_J \gg E_C = e^2/2C$ and when the bias current is slightly smaller than the critical current $I \lesssim I_0$. In this regime the last two terms in H can be accurately approximated by a cubic potential $U(\delta)$ parametrized by a barrier height $\Delta U(I) = (2\sqrt{2}I_0\Phi_0/3\pi)[1 - I/I_0]^{3/2}$ and a quadratic curvature at the bottom of the well that gives a classical oscillation frequency $\omega_p(I) = 2^{1/4}(2\pi I_0/\Phi_0 C)^{1/2}[1 - I/I_0]^{1/4}$.

The commutation relation leads to quantized energy levels in the cubic potential. The quantized energy levels in this potential can be visualized as indicated by Fig. 1a. Microwave bias currents induce transitions between levels at a frequency $\omega_{mn} = E_{mn}/\hbar = (E_m - E_n)/\hbar$, where E_n is the energy of state $|n\rangle$. The two lowest transitions have frequencies

$$\omega_{10} \simeq \omega_p\left(1 - \frac{5}{36}\frac{\hbar\omega_p}{\Delta U}\right) \text{ and} \qquad (2)$$

$$\omega_{21} \simeq \omega_p\left(1 - \frac{10}{36}\frac{\hbar\omega_p}{\Delta U}\right). \qquad (3)$$

These two frequencies must be different to access the two-state system as a controllable qubit. The ratio $\Delta U/\hbar\omega_p$ parameterizes the anharmonicity of the cubic potential with regard to the qubit states, and gives an estimate of the number of states in the well.

The state of the qubit can be controlled with a dc bias current I_{dc} and a time-varying bias current $I_{\mu w}(t)$ at frequency $\omega = \omega_{10}$, given by

$$I(t) = I_{dc} + \Delta I(t) \qquad (4)$$
$$= I_{dc} - I_{\mu w}(t)\cos(\omega t + \phi). \qquad (5)$$

In general, the Hamiltonian for the lowest three energy eigenstates of a Josephson junction system biased with a current $I(t)$ is

$$H = \begin{bmatrix} E_0 & 0 & 0 \\ 0 & E_1 & 0 \\ 0 & 0 & E_2 \end{bmatrix} \qquad (6)$$

$$+ \frac{\Phi_0}{2\pi}\Delta I \begin{bmatrix} \langle 0|\hat{\delta}|0\rangle & \langle 0|\hat{\delta}|1\rangle & \langle 0|\hat{\delta}|2\rangle \\ \langle 1|\hat{\delta}|0\rangle & \langle 1|\hat{\delta}|1\rangle & \langle 1|\hat{\delta}|2\rangle \\ \langle 2|\hat{\delta}|0\rangle & \langle 2|\hat{\delta}|1\rangle & \langle 2|\hat{\delta}|2\rangle \end{bmatrix}. \qquad (7)$$

The matrix elements $\langle m|\hat{\delta}|n\rangle$ are calculated as follows. When $I = I_{dc}$ and for $I_{dc} \to I_0$, the system Hamiltonian has a potential $U(\hat{\delta})$ that is cubic. We calculate this Hamiltonian, and solve for its eigenstates via diagonalization, from which the matrix elements $\langle m|\hat{\delta}|n\rangle$ can be simply computed. Calculating $\langle m|\hat{\delta}|n\rangle$ in this manner, we obtain

$$H \approx \begin{bmatrix} E_0 & g(t)e^{i(\omega t+\phi)} & 0 \\ g(t)e^{-i(\omega t+\phi)} & E_1 & \sqrt{2}g(t)e^{i(\omega t+\phi)} \\ 0 & \sqrt{2}g(t)e^{-i(\omega t+\phi)} & E_2 \end{bmatrix} + H_{nr}, \qquad (8)$$

where the basis states are $|0\rangle$, $|1\rangle$, and $|2\rangle$, from left to right, ω is the frequency of the applied time-varying current, and $g(t) = 1.014I_{\mu w}(t)\sqrt{\hbar/2\omega_{01}C}/2$ is related to the time-varying current $I_{\mu w}(t)$. A shaped pulse is implemented by letting $g(t)$ vary in time according to the amplitude modulation. The Hamiltonian H_{nr} contains additional diagonal and off-diagonal elements, but they are all sufficiently far enough off-resonance from ω_{10} and ω_{21} such that H_{nr} has only negligible effects.

To calculate the effect of amplitude modulation it is convenient to move into a doubly rotating frame, defined by the unitary operator

$$V = \begin{bmatrix} 1 & 0 & 0 \\ 0 & e^{i\omega t} & 0 \\ 0 & 0 & e^{2i\omega t} \end{bmatrix} \qquad (9)$$

Let $|\phi\rangle = V|\psi\rangle$ be a state in the rotating frame of V and $|\psi\rangle$ is a state in the laboratory frame. Then the equation of motion for this state can be derived from Schrödinger's Equation:

$$i\hbar\partial_t|\phi\rangle = \tilde{H}|\phi\rangle \qquad (10)$$

where $\tilde{H}$ is the rotating frame Hamiltonian given by $\tilde{H} = V^\dagger H V - i\hbar V^\dagger \partial_t V$. This results in

$$\tilde{H} = \begin{bmatrix} 0 & g(t)e^{i\phi} & 0 \\ g(t)^{-i\phi} & E_1 - \hbar\omega & \sqrt{2}g(t)e^{i\phi} \\ 0 & \sqrt{2}g(t)e^{-i\phi} & E_2 - 2\hbar\omega \end{bmatrix}, \quad (11)$$

where we have set $E_0 = 0$. In this work, we focus only on excitation that is on-resonance with the $|0\rangle \leftrightarrow |1\rangle$ transition. Using $E_1 = \hbar\omega_{10}$, $\omega = \omega_{10}$, and defining the energy difference between the two transitions as $E_2 - 2E_1 = \hbar\delta_\omega$, we obtain

$$\tilde{H} = \begin{bmatrix} 0 & g(t)e^{i\phi} & 0 \\ g(t)^{-i\phi} & 0 & \sqrt{2}g(t)e^{i\phi} \\ 0 & \sqrt{2}g(t)e^{-i\phi} & \hbar\delta_\omega \end{bmatrix}, \quad (12)$$

We can now use this rotating frame Hamiltonian in a straightforward manner to numerically calculate the effect of hard (square wave) and shaped pulses on the three-level system. We first discretize the shape to many steps. During each slice j, we let the amplitude of g be a constant, g_j. The unitary evolution in each slice is given by $U = \exp(-i\tilde{H}_j\Delta t/\hbar)$ where Δt is the slice length. We then vary g_j from slice to slice according to the modulation, and multiply all unitary evolutions together to obtain the overall evolution of the system, mathematically described as:

$$U = \prod_j \exp\left(-\frac{i\Delta t}{\hbar}\begin{bmatrix} 0 & g_j e^{i\phi} & 0 \\ g_j^{-i\phi} & 0 & \sqrt{2}g_j e^{i\phi} \\ 0 & \sqrt{2}g_j e^{-i\phi} & \hbar\delta_\omega \end{bmatrix}\right). \quad (13)$$

From U we can calculate the leakage out of the qubit manifold. Also note from Eq. 12 that the effects of δ_ω scale as the product $t\delta_\omega/2\pi$; the relevant normalized time unit in our problem is $\tau_{pw} = t\delta_\omega/2\pi$, and thus our results are plotted in this way.

III. SHAPED PULSES

Shaped pulses are widely used in Nuclear Magnetic Resonance (NMR) spectroscopy and NMR quantum computing[12–14] because they can significantly enhance the selective excitation of a qubit compared with hard pulses. In contrast to NMR, however, where each qubit is represented by a spin-1/2 particle, here the two transitions share an energy level, leading to system dynamics which are much more complex. Although it is not immediately obvious in what way amplitude modulating could be beneficial in this system, it is not unreasonable to assume that some improvements are possible. This assumption will be supported by our findings, later in this section.

In our simulations, we chose a flip angle of 180°, which transforms $|0\rangle \mapsto |1\rangle$ and $|1\rangle \mapsto |0\rangle$, because this is usually the hardest selective rotation to achieve. Even though we show results for several pulse shapes, we only provide explicit functions of the time dependence of $g(t)$ for Gaussian and Hermite 180 shapes. The RF envelope $g(t)$ of the Gaussian shape is given by:

$$g_{gauss}(t) = (a/t_g)\exp(-t^2/2t_g^2) \quad (14)$$

for $|t| < \alpha t_g$ and $g(t) = 0$ otherwise, where α is the cutoff of the pulse in time (usually 3-5), a is the amplitude ($a \approx 1.25$ for 180° pulses and for typical values of α), and t_g is the characteristic pulse width. The total pulse width is $t_{pw} = 2\alpha t_g$.

The Hermite 180 shape[15] is simply a Gaussian multiplied by a second order polynomial. The RF envelope $g(t)$ of the Hermite 180 shape is

$$g_{hrm180}(t) = (1 - \beta(t/\alpha t_g)^2)(a/t_g)\exp(-t^2/2t_g^2), \quad (15)$$

with the definition of parameters as before. The parameter β determines how strongly the Gaussian pulse is modulated. Here, $a \approx 2.2$ for $\alpha = 3$ and $a \approx 1.67$ for $\alpha = 4$, both for $\beta = 4$ and a 180° flip angle.

Using these parameters and shapes we have calculated the performance of the pulses. We define the error as $\epsilon = 1 - |U(3,3)|^2$ where $U(3,3)$ denotes the $(3,3)$ element of the resulting unitary transform. Ideally, $\epsilon = 0$ if we are only operating on the desired qubit subspace. Otherwise, the undesired energy level is involved in the operation. The error ϵ is the same as the maximum probability of being in the state $|2\rangle$ after the application of the pulse, when starting from an arbitrary superposition of $a|0\rangle + b|1\rangle$. The measure ϵ serves as a lower bound error because in addition to leakage outside the qubit manifold, the desired qubit rotation may also slightly deviate from the ideal rotation even when $\epsilon = 0$. For example, one deviation is due to transient Bloch-Siegert shifts, similar to NMR[16,17], but these effects can be corrected using a method similar to the one described in ref. 18.

We can numerically calculate the error via Eq. 13, but in order to gain an intuitive understanding of which time-dependent amplitude modulation could be most useful, it is helpful to estimate the error first, using a more conventional method based on simple bandwidth considerations. This system's response is approximately linear
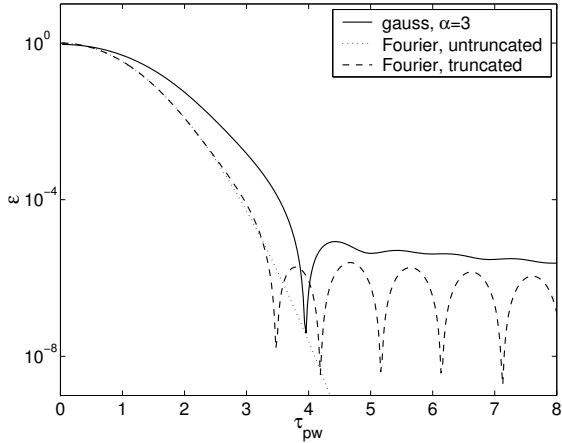
FIG. 2: Numerical calculation of the error ϵ as a function of normalized pulse width $\tau_{pw} = t_{pw}\delta_\omega/2\pi = 2\alpha t_g\delta_\omega/2\pi$ via Fourier analysis using the untruncated and truncated Gaussian shape, compared with the exact calculation.

FIG. 3: Plot of the error ϵ as a function of the normalized pulse width τ_{pw} for three different pulse shapes and several different levels of truncation.

FIG. 4: Plot of the error ϵ as a function of normalized pulse width τ_{pw} for several traditional NMR pulse shapes. The Gaussian shape here corresponds to $\alpha = 3$ from Fig. 3.

for small rotation angles, and hence Fourier analysis provides useful insight. In fact, Fourier analysis has been used extensively in NMR even for large rotation angles in order to get a first idea of the selectivity of a shaped pulse.

The relative power of the frequency component of the untruncated Gaussian shaped pulse at a frequency δ_ω away from ω_{10} is given by

$$\epsilon(\tau_{pw}) \approx \exp\left(-(\delta_\omega t_g)^2\right) = \exp\left(-\left(\frac{\pi\tau_{pw}}{\alpha}\right)^2\right). \quad (16)$$

This is plotted in Fig. 2 and is compared with both the Fourier analysis of a truncated Gaussian shaped pulse and the exact calculation using Eq. 13. For small pulse widths, the exact calculation and the one based on the Fourier analysis of untruncated shapes are similar, but the exact calculation flattens out for $\tau_{pw} > 4$. Though approximate, it is evident that Fourier analysis still provides a rough estimate of the error, especially if truncation effects are included. From Fourier analysis we expect hard pulses to perform poorly compared with Gaussian or Hermite shapes. In order to quantify the performance accurately however, we must calculate the error exactly using Eq. 13.

Fig. 3 plots ϵ as a function of the normalized pulse width for hard, Gaussian and Hermite shaped pulses. Clearly, for low error rates, a long pulse must be used. Since our goal is to apply the desired rotation as quickly as possible, it appears that the Gaussian shape is best suited for this problem. Also, the Gaussian shape could probably be further optimized using our calculational methods outlined here.

There exist other pulse shapes which have been designed for NMR experiments to invert or select spins over a very sharp and specified bandwidth. These belong to the class of BURP (Band-selective, Uniform-Response, Pure-phase) pulses[19], and their performance
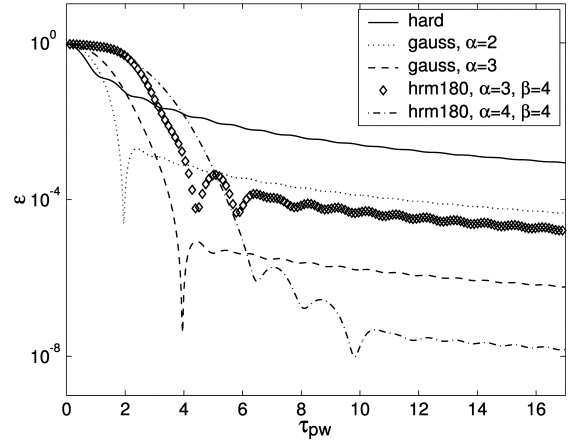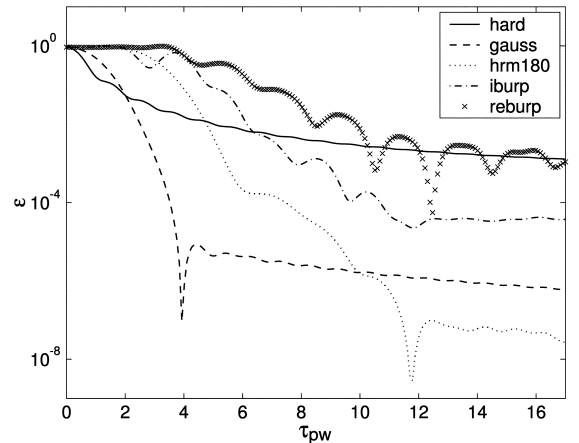
is shown in Fig. 4 compared with hard, Gaussian and Hermite shapes. Rather surprisingly, these specially designed shapes perform rather poorly in our three-level system.

It is also interesting to note that the error ϵ (or the maximum occupation probability of state $|2\rangle$) *during* the application of the pulse may be much higher than at the end of the pulse, as indicated in Fig. 5. Depending on the experiment, this may still be undesirable, for example when the lifetime of the third energy level is short. We discuss the impact of such short lifetimes later, in section V.

While pulse shaping clearly offers advantages in this three-level system, it may not necessarily be straightforward to do so experimentally, and hence it is useful to look at alternatives to pulse shaping. In the next section we discuss how composite pulses could provide an alternative approach towards improving single-qubit op-
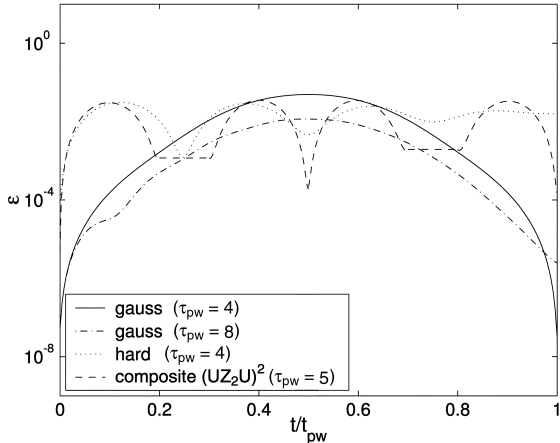
FIG. 5: Plot of the error ϵ (maximum occupation probability) as a function of time normalized with respect to the total pulse length t_{pw} during a hard and Gaussian shaped pulse and the second composite pulse (section IV. B.). A Gaussian-shaped pulse with a pulse width of $\tau_{pw} = 4$ has a very small error (about 10^{-8}), but *during* the pulse the error can be as high as 5 x 10^{-2}. The error during the pulse can be reduced by applying the pulse for a longer duration since the maximum error scales as approximately $1/\tau_{pw}$, based on Fourier analysis of the truncated pulses.

erations in a Josephson phase qubit.

IV. COMPOSITE PULSES

A composite pulse is a pulse that consists of a sequence of individual pulses, and is designed to reduce certain types of errors, but often at the cost of longer total duration. The individual pulses are typically square wave pulses, but can in principle be shaped pulses as well. Similar to shaped pulses, composite pulses have also found a wide variety of applications in NMR[12,20,21]. The overall unitary evolution U of a composite pulse is calculated via $U = \prod_k U_k$, where the U_k are the unitary evolutions of the individual pulses contained in the sequence. We next describe the design of two different composite pulses, both of which perform better than hard pulses.

A. Composite pulses - method 1

We begin by noting that $g = 0$ is a valid choice for a pulse. This corresponds to applying no electromagnetic radiation for some time. Working with the rotating frame Hamiltonian of Eq. 12, and letting the quantum system freely evolve for a time $t = \pi/\delta_\omega$, we obtain the transformation:

$$Z_2 = \begin{bmatrix} 1 & 0 & 0 \\ 0 & 1 & 0 \\ 0 & 0 & -1 \end{bmatrix}, \qquad (17)$$

where the subscript denotes that state $|2\rangle$ acquires a $180°$ phase shift with respect to all other states. Now, if we sandwich a driven evolution $U(t)$ between two free evolution periods Z_2, we obtain

$$
\begin{aligned}
V(t) &= Z_2 U(t) Z_2 \\
&= \exp\left(-\frac{it}{\hbar} \begin{bmatrix} 0 & g & 0 \\ g & 0 & -\sqrt{2}g \\ 0 & -\sqrt{2}g & \hbar\delta_\omega \end{bmatrix} \right), \quad (18)
\end{aligned}
$$

where we assumed g to be real and $U(t) = e^{-i\tilde{H}t/\hbar}$. Note that we can interpret the exponent of $V(t)$ as applying an $\hat{x}$-rotation on the $|0\rangle \leftrightarrow |1\rangle$ transition and a *negative* $\hat{x}$-rotation on the $|1\rangle \leftrightarrow |2\rangle$ transition, in the limit of fast pulses ($\delta_\omega/g \to 0$). If we now apply a second pulse $U(t)$ which can be regarded as an $\hat{x}$-rotation on both transitions, the excitation of the undesired transition is undone. The overall transformation is then given by $W(t) = U(t/2)V(t/2) = U(t/2)Z_2 U(t/2)Z_2$, and is an interesting pulse sequence because it becomes a nontrivial unitary transform on just the desired qubit manifold in the limit of fast pulses with $g \gg \delta_\omega$.

This procedure, however, only works for small rotation angles. Even though the interpretation of the *exponents* of $V(t)$ and $U(t)$ above is correct, the matrices $V(t)$, $U(t)$, and $W(t)$ themselves have elements connecting the $|0\rangle$ and $|2\rangle$ states whose magnitudes are second order in time t. We can only ignore these for small rotation angles. For larger rotation angles, one may have to apply a sequence of $W(t/n)$,

$$R(t) = [W(t/n)]^n \qquad (19)$$

to suppress the $|0\rangle \leftrightarrow |2\rangle$ excitation. Furthermore, if we chose n sufficiently large, then state $|2\rangle$ also only has a very small transient population *during* the pulse sequence. The total operation time is equal to $n(2\pi/\delta_\omega)+\tau$ (where τ is the total duration of the electromagnetic radiation), which becomes quite long for large n. Surprisingly, this composite method still performs rather well even when the system is far away from the short pulse limit $g \gg \delta_\omega$, as shown in Fig. 6.

B. Composite pulses - method 2

Another composite pulse design is based on the previous solution, supplemented by Bloch-sphere intuition and knowledge about the excitation profile of a hard pulse.

Suppose we excite a two-level system $\delta_\omega/2\pi$ hertz away from resonance via a hard pulse of duration τ. Whenever $\delta_\omega/2\pi$ is an integer multiple of $1/\tau$, the system is not excited. However, in our system the two transitions share an energy level. Hence, even if we excite the undesired transition off-resonance, there is still a substantial error, as evident from Fig. 3. Nonetheless, such a carefully timed pulse is still useful for the design of our composite pulse.

For the first step of the composite pulse, let the hard pulse be applied on resonance with the $|0\rangle \leftrightarrow |1\rangle$ transition for a time of $2\pi/\delta_\omega$. Let this pulse be denoted by $U(2\pi/\delta_\omega)$ and let the power be such that we would obtain only a small rotation angle (less than $45°$). The resulting matrix element of $U(2\pi/\delta_\omega)$ connecting the $|1\rangle$ and $|2\rangle$ states is very small because this transition is $\delta_\omega/2\pi$ Hz off-resonance, in accordance with our Fourier intuition from the previous paragraph. However, $U(2\pi/\delta_\omega)$ still has a matrix element connecting the $|0\rangle$ and $|2\rangle$ states because the two transitions share an energy level, leading to errors (similar to $U(t)$ and $V(t)$ from above). The last step of the composite pulse simply consists of undoing the $|0\rangle \leftrightarrow |2\rangle$ excitation.

The $|0\rangle \leftrightarrow |2\rangle$ excitation can be reversed by using the fact that a $180°$ $\hat{z}$-rotation sandwiched between two $\hat{x}$-rotations leads to no net excitation. Suppose we apply the sequence $C = U(2\pi/\delta_\omega)Z_2U(2\pi/\delta_\omega)$. Let us investigate the effects of C on the three possible excitations: (1) The first and last pulses, $U(2\pi/\delta_\omega)$, excite the $|0\rangle \leftrightarrow |1\rangle$ transition, whereas Z_2 has no effect on the states $|0\rangle$ and $|1\rangle$. (2) Neither $U(2\pi/\delta_\omega)$ nor Z_2 excite the $|1\rangle \leftrightarrow |2\rangle$ transition as described in the previous paragraph. (3) The two pulses $U(2\pi/\delta_\omega)$ lead to excitations between the states $|0\rangle$ and $|2\rangle$, which can be regarded as $\hat{x}$-rotations, whereas Z_2 acts like a $180°$ $\hat{z}$-rotation on the same states. Hence, the sequence C leads to no net excitation between the $|0\rangle$ and $|2\rangle$ states.

As a result, the sequence C acts non-trivially only on the desired qubit manifold. By carefully adjusting the power of the pulses we can create any arbitrary $\hat{x}$-rotation on the desired transition. The sequence thus consists of the application of two pulses of length $2\pi/\delta_\omega$ interlaced with a free evolution of length π/δ_ω.

Similar to the previous composite pulse, this method results in low errors ϵ only when $U(2\pi/\delta_\omega)$ implements small rotations. Hence in general, we may also have to apply n instances of $U(2\pi/\delta_\omega)Z_2U(2\pi/\delta_\omega)$ if our goal is to achieve large rotation angles. The resulting duration of this composite pulse is $2.5n(2\pi/\delta_\omega)$.

Fig. 6 shows the results of the composite pulse methods compared to a hard pulse and the Gaussian shaped pulse. The time axis denotes the *total* duration of the pulses. For the composite pulses, this includes the duration of the electromagnetic radiation plus the delay period implementing Z_2. As can be seen, the two composite pulse methods outperform hard pulses but not a Gaussian pulse with $\alpha = 3$. It is clear that the two simple composite pulses may provide useful alternatives for implementing accurate single qubit rotations in a Josephson phase qubit. Furthermore, it should be possible to combine shaped and composite pulses to even further improve qubit operations.

Nonetheless, as is the case with shaped pulses, the occupation probability of state $|2\rangle$ during the application of the composite pulse can be rather large. For the second composite pulse, this number is 3 x 10^{-2} (see Fig. 5), which is much larger than the occupation probabil-
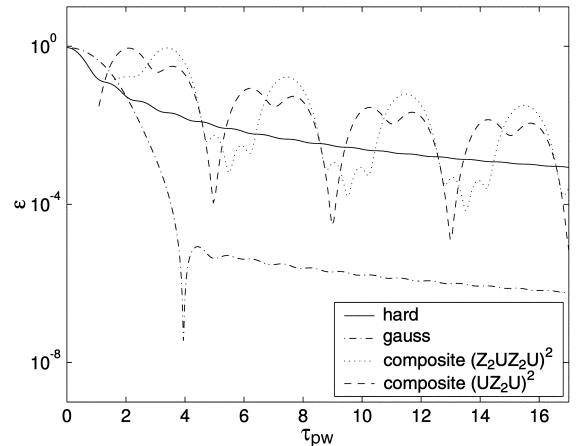
FIG. 6: Plot of the error ϵ as a function of normalized total time τ_{pw} for the two composite pulses ($n = 2$) described in section IV., compared with a hard and Gaussian shaped pulse. The first composite method outperforms hard pulses whenever the pulses are multiples of $2\pi/\delta_\omega$ even though the limit of $g \gg \delta$ does not apply here. For the second composite pulse, when the applied pulses are integer multiples of $2\pi/\delta_\omega$, the error is minimized as expected.

ity at the end of the pulse. In the next section we show how transient populations in the third energy level can be highly undesirable in the presence of high tunneling rates.

V. EFFECTS OF TUNNELING

Thus far we have only considered the ideal case where the two transitions of the three-level system are close in frequency but otherwise there exist no sources of decoherence. However, in a real Josephson phase qubit, the quantum state can tunnel through the barrier of the cubic well, and this process acts as a source of decoherence. What consequences do we expect from this?

From first principles we know that the tunneling rate depends exponentially on the barrier height and width. Hence in our cubic potential, we expect the upper level to be most susceptible to tunneling. When the tunneling rate out of this energy level is high, then there exists a significant source of decoherence if the state becomes even transiently populated. It is thus desirable to keep transient populations in state $|2\rangle$ as small as possible *during* our single qubit rotations. This may not necessarily be the case however, as indicated in Fig. 5. We next estimate the impact of this tunneling effect, first by using a simple model, followed by a more rigorous approach.

A. A simple tunneling model

A first model that gives insight into the importance of transient populations during the pulses can be set up
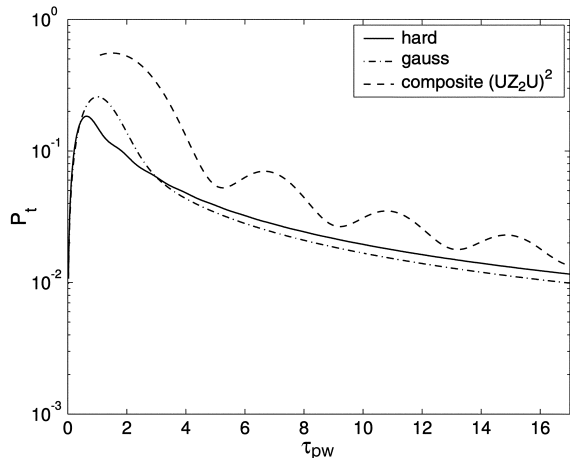
FIG. 7: Plot of P_t as a function of normalized pulse width for a hard, Gaussian and composite pulse taking $\Gamma_2 \approx \delta_\omega/2\pi \approx (\omega_{10}/2\pi)/100$. Clearly, the estimate of the tunneling probability is several orders of magnitude higher than ϵ, indicating that tunneling effects are important.

as follows. Let the probability of being in state $|2\rangle$, and the tunneling rate out of $|2\rangle$ be defined as p_2 and Γ_2 respectively. The probability of tunneling out of state $|2\rangle$ can then be calculated by $P_t = \int p_2 \Gamma_2 dt$. If we bias the system such that Γ_2 is on the order of $\delta_\omega/2\pi$, which is about 10 times larger than the inverse of typical pulse widths[5], we expect any transient populations in state $|2\rangle$ to tunnel out of the potential well during the pulse. Since the tunneling rates out of $|1\rangle$ (Γ_1) and $|0\rangle$ (Γ_0) are about 10^3 and 10^6 times less than Γ_2, we ignore their effects in this simple calculation[5].

In Fig. 7 we plot P_t as a function of normalized pulse width for a hard, Gaussian, and the second composite pulse with a tunneling rate $\Gamma_2 \approx (\omega_{10}/2\pi)/100 \approx \delta_\omega/2\pi$. Clearly, the error is several orders of magnitude higher than ϵ, and tunneling thus appears to be an important source of decoherence for this system, as expected. Note that P_t is only an approximate overall error because it reflects only the probability of tunneling and does not include the occupation probability of being in state $|2\rangle$ at the end of the pulse, which can be non-zero regardless of the tunneling rate. We next describe a more rigorous approach that analyzes the effects of tunneling and includes the leftover occupation probability of state $|2\rangle$.

B. A tunneling model using the operator-sum representation

We shall model the tunneling behavior similar to amplitude damping by using the operator-sum representation[22]. This type of model has been successfully used to predict the impact of decoherence in several NMR quantum computing experiments[14,23]. In the operator sum representation, an initial density matrix ρ_i is

mapped to a final density matrix ρ_f via

$$\rho_f = \sum_k E_k \rho_i E_k^\dagger, \tag{20}$$

where $\sum_k E_k^\dagger E_k = I$ and E_k are the Kraus operators[22]. For amplitude damping acting on a single qubit, we have only two Kraus operators, taking the form

$$E_0 = \begin{bmatrix} 1 & 0 \\ 0 & \sqrt{1-P_\Gamma} \end{bmatrix} \text{ and} \tag{21}$$

$$E_1 = \begin{bmatrix} 0 & \sqrt{P_\Gamma} \\ 0 & 0 \end{bmatrix}, \tag{22}$$

where $P_\Gamma = 1 - e^{-t\Gamma}$ with Γ denoting the inverse lifetime of the $|1\rangle$ state. From this, it becomes clear that any quantum state eventually collapses to the ground state $|0\rangle$.

The tunneling mechanism out of state $|2\rangle$ is now modeled by using a fourth, fictional auxiliary energy level $|T\rangle$ which acts as a reservoir for the tunnel states. We now define a fictitious qubit with basis states $|2\rangle$ and $|T\rangle$. The tunneling mechanism from $|2\rangle$ to the auxiliary level is then captured by modeling amplitude damping on the fictitious qubit. In this case the two Kraus operators take the form

$$E_0 = \begin{bmatrix} 1 & 0 & 0 & 0 \\ 0 & 1 & 0 & 0 \\ 0 & 0 & \sqrt{1-P_\Gamma} & 0 \\ 0 & 0 & 0 & 1 \end{bmatrix}, \text{ and} \tag{23}$$

$$E_1 = \begin{bmatrix} 0 & 0 & 0 & 0 \\ 0 & 0 & 0 & 0 \\ 0 & 0 & 0 & 0 \\ 0 & 0 & \sqrt{P_\Gamma} & 0 \end{bmatrix} \tag{24}$$

with the basis states $|0\rangle$, $|1\rangle$, $|2\rangle$, and $|T\rangle$ going from left to right. These operators also ensure that if the state tunneled, then all coherences to that state vanish. For example, if the initial state was an equal superposition of $|0\rangle$ and $|2\rangle$, then after tunneling we have a mixed state without coherences, and find that the system is in state $|0\rangle$ or $|T\rangle$, each with probability 0.5.

The tunneling rates Γ_1 and Γ_0 are $\sim 10^3$ and $\sim 10^6$ times lower than Γ_2, as described earlier. When $\Gamma_2 \approx \delta_\omega/2\pi$, we estimate their contributions to be only on the order of 10^{-5} for typical pulse widths, using the simple tunneling model from above. Hence we do not include their effects in our operator-sum approach. Later, we show how to generalize our method to include tunneling from an arbitrary number of levels, and use this generalized method to verify that Γ_1 and Γ_0 are indeed negligible, though we do not explicitly show our results here.

The Kraus operators above describe the tunneling mechanism, but they do not include excitation effects. The next step to model the single-qubit rotations in the presence of tunneling is to include the excitation of the transitions due to the applied radiation. The excitations of the two transitions in our three-level system do not
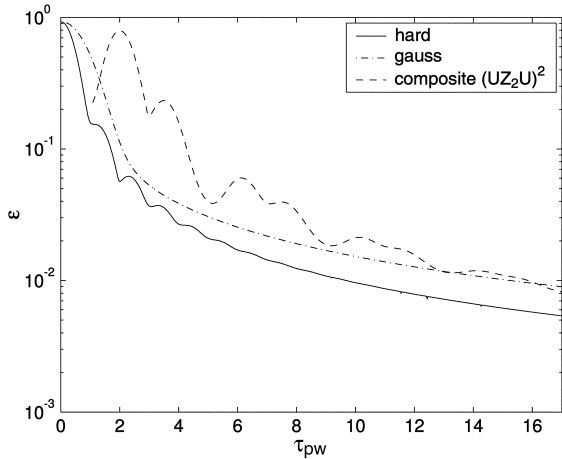
FIG. 8: Plot of the error as a function of normalized pulse width when including tunneling effects with $\Gamma_2 \approx \delta_\omega \approx (\omega_{10}/2\pi)/100$. The error is given by the maximum of $|2\rangle\langle 2| + |T\rangle\langle T|$ over all possible input superpositions $a|0\rangle + b|1\rangle$. Now, the hard pulse shows the best performance, but still with a large error.

commute with the tunneling mechanism. Thus, strictly speaking, one may have to derive a more complex formalism that captures both the tunneling effect and the qubit excitation simultaneously. However, we approximate the simultaneous behavior by slicing the microwave pulses into many discrete steps (as has been done in sections III and IV), and then simulate the tunneling and excitation one after the other in each step. In the limit as the number of steps goes to infinity this approximation becomes exact; we have used 256 steps for our simulation.

From Eq. 20, it becomes clear that the operator formalism takes density matrices as the input, which we have not yet specified. Our goal is to find the maximum possible error over all possible input states, which are arbitrary superpositions of the qubit, defined as $a|0\rangle + b|1\rangle$. We vary the values a and b to maximize the error, which is defined as the sum of the $|2\rangle\langle 2|$ and $|T\rangle\langle T|$ elements of the resulting density matrix. This corresponds to the maximum probability of being in the states $|2\rangle$ and $|T\rangle$. It is a useful error measure, and in the absence of tunneling it yields the *same* error ϵ that we have defined before.

In Fig. 8 we plot the error as a function of normalized pulse width for a tunneling rate $\Gamma_2 \approx \omega_{10}/100 \approx \delta_\omega/2\pi$. From this figure, we notice that the error is on the order of 10^{-2} for typical pulse widths. Note that especially for the Gaussian shaped pulse, the exact calculation matches the result of the simple tunneling model from Fig. 7 reasonably well. It is evident from both plots that for typical pulse widths the error is much larger than the 10^{-4} threshold required for fault-tolerant computations[24]. How can we reduce the error resulting from tunneling without significantly increasing the pulse widths?

From the simple theoretical model described earlier, the most straight forward method is to decrease the tunneling rates, which can be done by adjusting the bias current I to include more than three energy levels in the well. In this case, the frequency difference $\delta_\omega/2\pi$ between the transitions becomes slightly smaller. However, the tunneling rate is exponentially dependent on the barrier thickness, and thus we can reduce the tunneling rate by many orders of magnitude while only slightly decreasing the frequency difference between the transitions. With four levels in the well, we can reduce Γ_2 by three orders of magnitude to about $(\delta_\omega/2\pi)/1000$ while decreasing $\delta_\omega/2\pi$ by only 30%. Though Γ_3 is still high (about $\delta_\omega/2\pi$), level $|3\rangle$ is sparsely populated because the $|2\rangle \leftrightarrow |3\rangle$ transition is about $2\delta_\omega/2\pi$ Hz off-resonance and hence should not be significantly excited.

The tunneling effects from $|2\rangle$ and $|3\rangle$ during single-qubit rotations can be calculated via the operator-sum representation as follows. The effect of the radiation and tunneling acting simultaneously is approximated as before by slicing the pulse into many steps and simulating tunneling and excitation one after the other in each step. The tunneling is modeled by sequentially modeling tunneling out of states $|2\rangle$ and $|3\rangle$. In other words, we first apply the two Kraus operators that describe the tunneling from $|2\rangle$ to $|T\rangle$. Then, we apply the two Kraus operators that the describe the tunneling from $|3\rangle$ to $|T\rangle$. Strictly speaking this is not correct because the Kraus operators that describe tunneling from $|2\rangle$ do not commute with those describing the tunneling from $|3\rangle$. However, since the pulse is already discretized into many steps (we used 256), during each of which we model tunneling separately, our approach becomes a good approximation. The resulting four Kraus operators can be easily derived from Eqs. 23 and 24. Furthermore, we can model the tunneling from an arbitrary number of states in this manner, and have verified that the error for a three-level system is indeed dominated by the tunneling from state $|2\rangle$ and that tunneling from $|1\rangle$ and $|0\rangle$ is negligible.

Fig. 9 shows the error for a four level system with tunneling rates $\Gamma_2 \approx (\delta_\omega/2\pi)/1000$, and $\Gamma_3 \approx \delta_\omega/2\pi$. As can be seen, the results are much improved compared with Fig. 8. In fact, now the composite pulse can be as good as the Gaussian shaped pulse.

It is possible to continue increasing the number of levels in the well to suppress tunneling even further. However, this may not be practical much beyond four or five levels because the state measurement needs a transition between state $|1\rangle$ and a higher energy state with a very large tunneling rate[5]. This becomes increasingly difficult for more energy levels in the well. In the four level case, it is possible to directly excite the $|1\rangle \leftrightarrow |3\rangle$ transition[25].

Finally, we point out that other proposals for performing single qubit rotations in a three or multilevel system[6–8] are also problematic whenever energy levels with high tunneling rates are populated. We believe that our method for simulating the tunneling mechanism could be useful to estimate the feasibility of these and
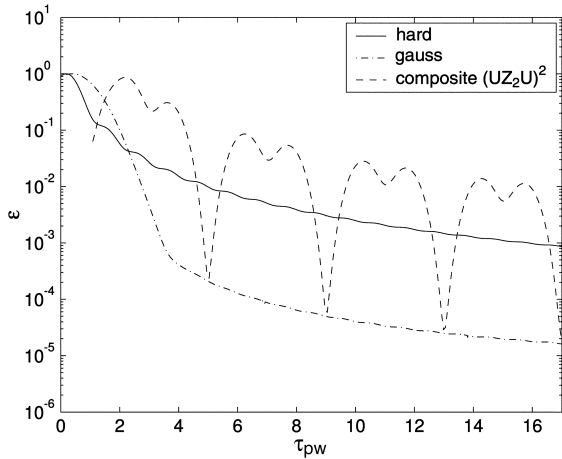
FIG. 9: Plot of the error as a function of normalized pulse width when including tunneling effects in a four level system. The tunneling rate Γ_2 is $(\delta_\omega/2\pi)/1000$, and Γ_3 is 1000 times higher. The error is given by $|2\rangle\langle 2| + |3\rangle\langle 3| + |T\rangle\langle T|$ after maximizing over all possible input superpositions $a|0\rangle + b|1\rangle$. In this case, the composite pulse can perform about as well as a Gaussian pulse.

other methods.

VI. CONCLUSIONS

In summary, we have shown how shaped and composite pulses can improve the accuracy of single-qubit operations in a Josephson phase qubit. We estimate the feasibility of our methods by including tunneling effects to show that tunneling can be a dominant source of decoherence, and we conclude that operating a Josephson phase qubit with three levels is not recommended. Instead, to reduce decoherence effects from unwanted tunneling one may wish to operate the system with four energy levels.

Typical junction parameters are $\omega_{10}/2\pi \approx 10$ GHz, $\Delta U/\hbar\omega_p \approx 4$, and $\delta_\omega \approx 0.04\omega_{10}$, leading to typical pulse widths t_{pw} that are on the order of a few nanoseconds or tens of nanoseconds. We believe that commercial electronics can be used to achieve accurate circuit timings which accommodate shaped and composite pulses at these time scales.

This work also takes first steps towards applying NMR quantum computing and spectroscopy techniques to related quantum systems, in particular the superconductor based qubit system. We believe that continued effort into this direction could prove fruitful for other implementations of quantum computers including solid state and trapped ion implementations. Furthermore, we applied fundamental ideas from quantum computing to simulate tunneling effects in Josephson junction qubits, illustrating how quantum computing is useful in modeling and simulating the physics of real quantum systems in a straightforward manner.

* Electronic address: msteffen@snowmass.stanford.edu

[1] M. A. Nielsen and I. L. Chuang, *Quantum computation and quantum information* (Cambridge University Press, Cambridge, 2000).

[2] J. I. Cirac and P. Zoller, Phys. Rev. Lett. **74**, 4091 (1995).

[3] Y. Nakamura, Y. A. Pashkin, and J. S. Tsai, Nature **398**, 786 (1999).

[4] Y. Yu, S. Han, X. Chu, S.-I. Chu, and Z. Wang, Science **296**, 889 (2002).

[5] J. Martinis, S. Nam, J. Aumentado, and C. Urbina, Phys. Rev. Lett. **89**, 117901 (2002).

[6] L. A. Wu and D. A. Lidar, arXive eprint quant-ph/0303129 (2003).

[7] L. Tian and S. Lloyd, Phys. Rev. A **62**, 050301 (2000).

[8] J. Palao and R. Kosloff, Phys. Rev. Lett. **89**, 188301 (2002).

[9] C. Bauer, R. Freeman, T. Frenkiel, J. Keeler, and A. Shaka, J. Magn. Reson. **58**, 442 (1984).

[10] N. Gershenfeld and I. L. Chuang, Science **275**, 350 (1997).

[11] J. Martinis, S. Nam, J. Aumentado, and K. Lang, Phys. Rev. B **67**, 094510 (2003).

[12] R. Freeman, *Spin Choreography* (Spektrum, Oxford, 1997).

[13] R. R. Ernst, G. Bodenhausen, and A. Wokaun, *Principles of Nuclear Magnetic Resonance in One and Two Dimensions* (Oxford University Press, Oxford, 1994).

[14] L. Vandersypen, M. Steffen, G. Breyta, C. Yannoni, R. Cleve, and I. L. Chuang, Nature **414**, 883 (2001).

[15] W. Warren, J. Chem. Phys. **81**, 5437 (1984).

[16] F. Bloch and A. Siegert, Phys. Rev. **57**, 522 (1940).

[17] L. Emsley and G. Bodenhausen, Chem. Phys. Lett. **168**, 297 (1990).

[18] M. Steffen, L. Vandersypen, and I. Chuang, J. Magn. Reson. **146**, 369 (2000).

[19] M. Green and R. Freeman, J. Magn. Reson. **93**, 93 (1991).

[20] M. Levitt and R. Freeman, J. Magn. Reson. **33**, 473 (1979).

[21] M. Levitt, Prog. NMR Spectrosc. **18**, 61 (1986).

[22] K. Kraus, *States, Effects, and Operations: Fundamental Notions of Quantum Theory*, Lecture Notes in Physics, Vol. 190 (Springer-Verlag, Berlin, 1983).

[23] M. Steffen, W. van Dam, T. Hogg, G. Breyta, and I. Chuang, Phys. Rev. Lett. **90**, 067903 (2003).

[24] A. M. Steane, arXive eprint quant-ph/0207119 (2002), URL http://www.arxiv.org/abs/quant-ph/0207119.

[25] R. Simmonds, K. Lang, D. Hite, D. Pappas, and J. Martinis, in preparation (2003).